Published in final edited form as:
Mol Cell. 2014 November 6; 56(3): 376–388. doi:10.1016/j.molcel.2014.09.011.

miR-14 regulates autophagy during developmental cell death by targeting *ip3-kinase 2*

Charles Nelson[1], **Victor Ambros**[2], and **Eric H. Baehrecke**[1,*]

[1]Department of Cancer Biology, University of Massachusetts Medical School, Worcester, MA 01605, USA

[2]Program in Molecular Medicine, University of Massachusetts Medical School, Worcester, MA 01605, USA

SUMMARY

Macroautophagy (autophagy) is a lysosome-dependent degradation process that has been implicated in age-associated diseases. Autophagy is involved in both cell survival and cell death, but little is known about the mechanisms that distinguish its use during these distinct cell fates. Here, we identify the microRNA, *miR-14*, as being both necessary and sufficient for autophagy during developmentally regulated cell death in *Drosophila*. Loss of *miR-14* prevented induction of autophagy during salivary gland cell death, but had no effect on starvation-induced autophagy in the fat body. Moreover, mis-expression of *miR-14* was sufficient to prematurely induce autophagy in salivary glands, but not in the fat body. Importantly, *miR-14* regulates this context-specific autophagy through its target, *inositol 1,4,5-trisphosphate kinase 2* (*ip3k2*) thereby affecting inositol 1,4,5-trisphosphate (IP3) signaling and calcium levels during salivary gland cell death. This study provides the first *in vivo* evidence of microRNA regulation of autophagy through modulation of IP3 signaling.

Keywords

autophagy; programmed cell death; microRNA; *miR-14*; IP3 kinase; IP3 signaling; calcium; *Calmodulin*

INTRODUCTION

Autophagy is a conserved catabolic process that delivers cytoplasmic materials, including proteins and organelles, to lysosomes for degradation (Mizushima and Komatsu, 2011). Autophagy functions in multiple cellular contexts, including infection, stress, and cell death, and is involved in multiple age-associated disorders, such as cancer and neurodegeneration.

*Corresponding author: Eric H. Baehrecke, Department of Cancer Biology, University of Massachusetts Medical School, Worcester, MA 01605 USA, telephone: 508-856-6733, fax: 508-856-1310, Eric.Baehrecke@umassmed.edu.

During starvation, cells utilize autophagy to maintain nutrient homeostasis and for cell survival. Autophagy can also function in cell death, such as in the developmentally regulated death of larval salivary gland cells in *Drosophila* (Berry and Baehrecke, 2007). Although much is known about the mechanisms that control autophagy in response to nutrient deprivation, little is known about the regulation of autophagy during developmental cell death.

microRNAs were first discovered as regulators of developmental timing; a process which appears to be conserved among metazoans (Ambros, 2011; Sokol, 2012). microRNAs are small, non-coding RNAs that primarily function by down-regulating gene expression post-transcriptionally through base pairing to the 3′untranslated regions (UTRs) of their target mRNAs. In *Drosophila*, microRNAs regulate multiple processes during development, including developmental timing, steroid hormone signaling, metabolism, and caspase activation (Brennecke et al., 2003; Caygill and Johnston, 2008; Varghese and Cohen, 2009; Varghese et al., 2010; Xu et al., 2003). The programmed degradation of larval salivary glands during *Drosophila* development requires the precise temporal regulation of hormone signaling, cell growth arrest, caspase activation, and autophagy (Berry and Baehrecke, 2007; Jiang et al., 1997; Lee and Baehrecke, 2001; Martin and Baehrecke, 2004). However, no microRNAs have been previously shown to control the destruction of this tissue.

microRNAs have been implicated in the regulation of autophagy (Frankel et al., 2011; Zhu et al., 2009). However, all previous studies have focused on the regulation of autophagy by microRNAs during nutrient deprivation in derived cell lines, and no evidence exists that microRNAs regulate autophagy under physiological conditions in animals. In addition, microRNAs have not been shown to influence autophagy during cell death, and how microRNAs influence autophagy is poorly understood.

Here we show that the microRNA, *miR-14*, is necessary for salivary gland degradation. While previous studies have shown that *miR-14* can regulate hormone signaling and caspase activity in other contexts, we find that *miR-14* does not influence either of these processes during salivary gland cell death. Rather, we ascertain that *miR-14* regulates autophagy in dying salivary gland cells, and does so by targeting *ip3k2*, a gene that is involved in inositol 1,4,5-trisphosphate (IP3) signaling and calcium release from the endoplasmic reticulum (ER). We determine that IP3 signaling, as well as the calcium binding messenger protein, Calmodulin, are necessary for the induction of autophagy during salivary gland cell death. In addition, through its regulation of *ip3k2*, *miR-14* is necessary for a rise in calcium levels coinciding with salivary gland death. Moreover, this regulation of autophagy by *miR-14*, IP3 signaling, and Calmodulin appears to be specific to the context of the developmental cell death of larval salivary glands, as starvation-induced autophagy in the larval fat body was not influenced by altered function of *miR-14*, *ip3k2*, IP3 signaling, or *Calmodulin*.

RESULTS

miR-14 functions in salivary gland cell death

The larval salivary glands of *Drosophila* undergo programmed cell death 14–16 hours after puparium formation resulting in no visible gland remnants by 24 hours after puparium

formation (described in Figures S1A and S1B). To determine if micoRNAs play a role in regulating salivary gland cell death, we inhibited microRNAs in the salivary gland by knocking down the microRNA processing factors *drosha* or *dicer-1* via salivary gland-specific RNAi. At 24 hours after puparium formation, histological analyses revealed that salivary gland cell fragments persisted in animals expressing a double-stranded inverse repeat construct designed to target either *drosha* (*drosha*^{IR}) or *dicer-1* (*dicer-1*^{IR}), but no residual salivary gland material was observed in control animals at the same stage (Figures 1A, 1B, S1E and S1F; emphasized in Figure S1C). We then determined the profile of microRNAs expressed in dying salivary glands (Table S1), and we screened 11 available mutants of gland-expressed microRNA genes for defects in salivary gland clearance. One null mutant, *miR-14*$^{\Delta 1}$, displayed a strong failure in salivary gland clearance (Figures 1C and 1D). In addition, expression of *miR-14* specifically in salivary glands of homozygous *miR-14* $^{\Delta 1}$ mutant animals rescued the degradation defect in this tissue (Figures 1C and 1D). Furthermore, expression of *drosha*^{IR} in the salivary glands of homozygous *miR-14* mutant animals failed to enhance the phenotype observed in *miR-14* mutant animals alone (Figures S1G and S1H). These results indicate that *miR-14* is required for salivary gland clearance, that *miR-14* functions in a salivary gland autonomous manner, and that if other microRNAs are required for salivary gland clearance, they function in the same genetic pathway as *miR-14*.

miR-14 does not regulate hormone signaling, cell growth arrest, or caspase activation during salivary gland cell death

Failure of salivary gland cell growth arrest results in attenuation of autophagy and incomplete salivary gland degradation (Berry and Baehrecke, 2007). Therefore, we tested if loss of *miR-14* influences salivary gland cell growth arrest by using the tGPH reporter for phosphatidylinositol-3,4,5-P3 (PIP3) activity (Britton et al., 2002), and by measuring cell area. We observed neither a difference in tGPH localization nor an increase cell area in control and *miR-14* mutant salivary glands (Figures 2A and 2B). These data indicate that the salivary gland degradation defect in *miR-14* mutant animals is not an indirect consequence of a defect in cell growth arrest.

Salivary gland cell death is triggered by a developmental rise in the steroid hormone 20-hydroxyecdysone (ecdysone) (Jiang et al., 1997). The Ecdysone Receptor (EcR) and its partner ultraspiracle (USP) then directly induce the transcription of multiple target genes including Broad Complex (BrC) leading to the degradation of the larval salivary glands (Gauhar et al., 2009). A previous study indicated that *miR-14* can influence EcR levels based on analyses of whole pupae 24 hours after puparium formation (Varghese and Cohen, 2009). Therefore, we tested if loss of *miR-14* influenced EcR and BrC levels during salivary gland death. To our surprise, neither EcR nor BrC protein levels were significantly altered in salivary glands by loss of *miR-14* (Figure 2C). These data indicate that the salivary gland clearance defect that is observed in *miR-14* mutant animals is not due to *miR-14* regulation of either EcR or altered steroid signaling.

Caspase activity and autophagy are both required for salivary gland degradation, and these two processes appear to function independently of each other (Berry and Baehrecke, 2007).

Thus, when either autophagy or caspases are inhibited, partial degradation of the salivary glands occurs resulting in a weaker degradation phenotype consisting of diffuse fragments of cellular material that we define as cell fragments. By contrast, when both caspases and autophagy are inhibited simultaneously, more intact tissue fragments in the shape of the two oval salivary glands persist resulting in a stronger phenotype that we define as gland fragments (described in Figures S1C and S1D) (Berry and Baehrecke, 2007). In *miR-14* homozygous mutant animals, we observed a weaker phenotype with dispersed cellular fragments (Figures 1C and 1D), suggesting that *miR-14* regulates either autophagy or caspase activity but not both.

Since *miR-14* was first identified as a genetic suppressor of apoptosis (Xu et al., 2003), we examined the relationship between caspases and *miR-14* in dying salivary glands. We expressed the caspase inhibitor p35 in the salivary glands of control and *miR-14* homozygous mutant animals. While the weaker phenotype of salivary gland cell fragments were observed in control animals of either p35-expressing or *miR-14* mutant alone, we observed a distinctly stronger phenotype of two large oval-shaped salivary gland tissue fragments in *miR-14* mutant animals that also expressed p35 (Figures 2D and 2E; emphasized in Figure S1D). This enhancement of the salivary gland clearance defect indicates that *miR-14* functions in an additive manner with the caspase pathway. In support of this conclusion, *miR-14* mutant and control salivary glands also exhibited no clear difference in either the timing or amount of cleaved Caspase-3 immuno-fluorescence (Figures 2F and 2G). Taken together, these data indicate that loss of *miR-14* does not influence caspases in dying salivary glands.

miR-14 is necessary and sufficient for autophagy during salivary gland cell death

Autophagy causes a reduction in cell size (Chang et al., 2013), and *miR-14* mutant salivary gland cells failed to shrink as much as control cells (Figure 2B) suggesting that autophagy may be defective in *miR-14* mutant salivary glands. To determine whether autophagy is involved in *miR-14* regulation of salivary gland cell death, we inhibited autophagy by knockdown of the autophagy gene *Atg6* in *miR-14* mutant animals. We observed no clear differences in the cell fragment phenotypes of *miR-14* homozygous mutant animals whether or not $Atg6^{IR}$ was expressed in salivary glands (Figures 3A and 3B). These data suggest that *miR-14* functions in the same pathway as *Atg6*, and, therefore, regulates salivary gland cell death by autophagy. Consistent with this interpretation, homozygous *miR-14* mutant salivary glands possess significantly fewer mCherry-*Atg8a* autophagy reporter puncta compared to heterozygous control salivary glands (Figures 3C and 3D). To determine if *miR-14* is a general regulator of autophagy, we tested if this miRNA is required for starvation-induced autophagy in the larval fat body. In contrast to salivary gland cell death, we observed no difference in the amounts of mCherry-*Atg8a* autophagy reporter puncta in the fat bodies of control versus homozygous *miR-14* mutant animals following four hours of nutrient deprivation (Figures 3E and 3F). This indicates that *miR-14* is necessary for developmentally regulated autophagy in the salivary gland, but is dispensable for starvation-induced fat body autophagy.

We next tested if *miR-14* is sufficient for autophagy. We observed that cell autonomous mis-expression of *miR-14* was sufficient to induce premature mCherry-*Atg8a* puncta in the salivary glands of third instar larvae (Figure 3G), but was not sufficient to induce autophagy reporter puncta in larval fat body (Figure 3H). To ensure that this tissue specific induction of autophagy was in fact because of mis-expression of *miR-14,* we repeated this experiment with a second *miR-14* transgenic line. Once again, autophagy was induced in the salivary gland, but not the fat body (Figures S2A and S2B). Thus, *miR-14* functions to regulate autophagy during developmental salivary gland cell death, but is not involved in nutrient deprivation-induced autophagy. The observation that mis-expression of *miR-14* resulted in autophagy occurring at an earlier developmental stage than in wild type (Figure 3G) suggests that during wild type development, *miR-14* levels may be limiting at earlier stages.

miR-14 targets the *ip3k2* gene to regulate autophagy during salivary gland cell death

Our next goal was to identify targets of *miR-14* that influence autophagy. We hypothesized that knockdown of *miR-14* targets would result in phenotypes that are similar to those induced by mis-expression of *miR-14.* Knockdown of either *EcR* or *sugarbabe,* two previously-identified targets of *miR-14* (Varghese and Cohen, 2009; Varghese et al., 2010), failed to induce mCherry-*Atg8a* autophagy reporter puncta in the salivary glands (Table S2). Therefore, we used the microRNA binding site prediction programs Pictar and Targetscan to identify candidate *mir-14* target genes, and then used RNAi lines against these candidate targets to screen for the induction of mCherry-*Atg8a* autophagy reporter puncta (Table S2). Of the 31 genes tested, only knockdown of *ip3k2* resulted in the tissue-specific induction of mCherry-*Atg8a* autophagy reporter puncta in salivary glands, and not in fat body (Figures 4A and 4B). To ensure that the phenotype observed was not due to an off target effect of the RNAi, we tested a second RNAi line that targeted a different sequence of *ip3k2*; this RNAi line also displayed the same phenotype as mis-expression of *miR-14* (Figures S3A and S3B).

To further validate *ip3k2* as a target of *miR-14* by genetic epistasis, we created a loss-of-function mutant, $ip3k2^{\Delta 1}$ (see Experimental Procedures) that lacks most of the *ip3k2* gene, including the conserved inositol polyphosphate kinase (IPK) domain (Figures S3C and S3D). When we combined the *ip3k2* and *miR-14* mutants we observed a significant suppression of the *miR-14* salivary gland clearance phenotype (Figures 4C and 4D). Furthermore, the *ip3k2* mutation suppressed the *miR-14* mutant salivary gland autophagy phenotype based on restoration of the number of mCherry-*Atg8a* autophagy reporter puncta (Figures 4E and 4F). Moreover, in *miR-14* mutant animals, we did not observe dominant suppression of the gland clearance phenotype nor restoration of mCherry-*Atg8s* puncta when animals were also heterozygous for the *ip3k2* mutation. In addition, the *ip3k2* mutant showed no difference in the number of mCherry-Atg8a puncta in fat bodies of either fed or nutrient deprived larvae (Figures S4A and S4B). Interestingly, we observed that deletion of *ip3k2* was sufficient to suppress the gland clearance phenotype observed when *drosha* was knocked down specifically in the salivary glands (Figures S5A and S5B). These data indicate that *ip3k2* functions genetically downstream of *miR-14* in the regulation of autophagy during salivary gland cell death, and that if other microRNAs regulate gland degradation, they appear to function upstream of and in the same pathway as *ip3k2*.

To investigate if *ip3k2* 3′ UTR sequences can mediate regulation by *miR-14*, we constructed *in vivo* green fluorescent protein (GFP) sensors. In these constructs, the 3′ UTR of *ip3k2* was fused to GFP creating a wild type control sensor, and a similar sensor was created with mutations in the predicted *miR-14* binding site (Figure S3E). Transgenic flies were generated containing either the wild type or mutant 3′ UTR constructs (Groth et al., 2004), and sensor levels were analyzed in control and *miR-14* mutant salivary glands by immuno-blot. With the wild type sensor, we observed a significant elevation of GFP protein in the salivary glands of homozygous *miR-14* mutant animals compared to the salivary glands of control animals (Figures 4G and 4H). Moreover, salivary gland GFP expression from the sensor containing the mutant *miR-14* binding site was increased in control animals, and was identical to the GFP levels in homozygous *miR-14* mutant animals (Figures 4G and 4H). These data support the conclusion that *ip3k2* is a bona fide direct target of *miR-14* that regulates autophagy during cell death of salivary glands.

IP3 signaling and Calmodulin are necessary for autophagy during salivary gland death

We next sought to determine how *ip3k2* regulates autophagy during salivary gland death. *ip3k2* contains a highly conserved IPK domain (Figure S4B) that is known to phosphorylate IP3 to form inositol 1,3,4,5-tetrakisphosphate (IP4) (Seeds et al., 2004). IP3 can serve as a cytoplasmic second messenger molecule that stimulates calcium release by binding the IP3-receptor, an ER localized calcium ion channel (Berridge et al., 2000).

We hypothesized that in *miR-14* mutant animals, IP3K2 levels are elevated resulting in low levels of IP3. To determine if IP3 signaling plays a role in salivary gland degradation, we expressed an IP3 sponge specifically in the salivary glands. This IP3 sponge contains multiple IP3 binding motifs that bind to IP3 and decrease its availability (Usui-Aoki et al., 2005). At 24 hours after puparium formation, the number of animals with persistent salivary gland cell fragments was increased in animals that expressed the IP3 sponge compared to control animals at the same stage (Figures 5A and 5B). In addition, expression of the IP3 sponge in salivary glands inhibited the induction of autophagy based on the number of mCherry-Atg8a puncta compared to controls (Figures 5C and 5D). Importantly, when the IP3 sponge was expressed in *ip3k2* mutant animals, we still observed the persistence of salivary gland cell fragments (Figures S5A and S5B) and low levels of mCherry-Atg8a puncta compared to controls (Figures 5E and 5F).

To complement our analyses of IP3 sponge expression, we also utilized RNAi to knock down the *ip3-receptor* specifically in the salivary glands. Similar to animals that express the IP3 sponge, animals with knockdown of the *ip3-receptor* in salivary glands possessed persistent salivary gland cell fragments (Figures 5G and 5H), and had significantly attenuated mCherry-Atg8a puncta compared to controls (Figures 5I and 5J). Furthermore, when the *ip3-receptor* was knocked down in *ip3k2* mutant animals, we still observed the persistence of salivary gland cell fragments (Figures S5C and S5D), and reduced mCherry-Atg8a puncta relative to controls (Figures 5K and 5L). However, when either the IP3 sponge was expressed or the *ip3-receptor* was knocked down with RNAi in the fat body of animals following nutrient deprivation, we observed no difference in the number of mCherry-Atg8a puncta compared to control cells (Figures S4C–S4F). These data indicate that IP3 signaling

through the IP3-receptor is necessary for autophagy and degradation during salivary gland cell death, but are dispensable for autophagy during nutrient deprivation of the fat body.

We hypothesized that IP3 regulates autophagy through calcium signaling during salivary gland cell death. To test our hypothesis, we used RNAi to decrease the function of the *Calmodulin* gene, which encodes a calcium-binding messenger protein. When *Calmodulin* was knocked down specifically in salivary glands we observed persistence of salivary gland cell fragments (Figures 6A and 6B), and decreased mCherry-Atg8a autophagy reporter puncta (Figures 6C and 6D). In addition, when *Calmodulin* was knocked-down specifically in the salivary glands of *ip3k2* mutant animals, the salivary gland cell fragments persisted (Figures 6E and 6F) and mCherry-Atg8a puncta were attenuated (Figures 6G and 6H). However, when *Calmodulin* was knocked down by RNAi in the fat body of nutrient deprived larvae, we observed no difference in the number of mCherry-Atg8a puncta compared to control cells (Figures S4G and S4H) indicating that *Calmodulin* is dispensable for autophagy during nutrient deprivation. Combined, these data indicate that Calmodulin functions downstream of IP3K2 in the regulation of autophagy during salivary gland cell death.

Next, we tested if IP3 signaling functioned downstream of *miR-14* as indicated by our previous experiments. When the *ip3-receptor* was knocked down simultaneously with mis-expression of *miR-14* in the salivary glands, we did not observe the premature increase in mCherry-*Atg8a* puncta characteristic of *mir-14* misexpression alone (Figures S7A and S7B; compare with Figure 3G). These data indicate that knockdown of the *ip3-receptor* is sufficient to suppress the induction of autophagy that is triggered by mis-expression of *miR-14*, and functions downstream of *miR-14*.

miR-14 and *ip3k2* influence calcium levels in the salivary gland

We hypothesized that *miR-14* regulation of *ip3k2* mediates release of calcium during salivary gland destruction. Therefore, we sought to determine if *miR-14* and *ip3k2* influence calcium levels in the salivary gland using the calcium indicator, GCaMP (Akerboom et al., 2012). Perturbations, such as dissection of the salivary gland, resulted in a rapid release of calcium. Therefore, we live-imaged salivary glands expressing GCaMP in intact animals. In control animals, an increase in the GCaMP signal was observed at eight hours after puparium formation coinciding with the rise in ecdysone that triggers salivary gland destruction (Figure 7). In *miR-14* mutant animals, the GCaMP signal was lower at all stages compared to control animals, including no marked increase at eight hours after puparium formation (Figures 7A and 7B). Additionally, *ip3k2* mutant animals exhibited a significant premature elevation in the GCaMP signal compared to control animals (Figures 7C and 7D). These data indicate that release of calcium precedes salivary gland death, *miR-14* is necessary for this release of calcium, and loss of *ip3k2* results in premature elevation of calcium.

DISCUSSION

While much is known about the regulation of autophagy during nutrient deprivation, relatively little is understood about the regulation of autophagy in the context of

programmed cell death. Our findings reveal a mechanism involving the regulation of *ip3k2* by the microRNA *miR-14*. In turn, these factors influence IP3 signaling and Calmodulin as a mechanism that distinguishes between the utilization of autophagy during programmed cell death from the use of autophagy in the context of cellular stress.

Previous studies have linked microRNAs and autophagy. For example, autophagy can modulate the intracellular levels of microRNAs by degradation of core microRNA machinery (Gibbings et al., 2012; Zhang and Zhang, 2013). In addition, multiple studies have shown that over-expression of microRNAs can be sufficient to inhibit autophagy in cell lines under starvation conditions (Frankel et al., 2011; Zhu et al., 2009). By contrast, our findings demonstrate that the microRNA, *miR-14*, is both necessary and sufficient for autophagy during developmental cell death in an animal, but that *miR-14* has no apparent effect on autophagy triggered by nutrient deprivation. While *miR-14* is expressed in the fat body (Varghese et al., 2010), it appears not to matter if *miR-14* regulates *ip3k2* in this tissue, as IP3 signaling and Calmodulin appear to play no detectable role in regulating autophagy during nutrient deprivation.

Interestingly, steroid signaling and caspase activity are both necessary for salivary gland cell death, and in other contexts, these two processes have been shown to be regulated by *miR-14* (Varghese and Cohen, 2009; Varghese et al., 2010; Xu et al., 2003). However, during salivary gland cell death, neither of these processes was affected by loss of *miR-14*. This new role of *miR-14* in promoting organ-specific developmental autophagy underscores the context-specific roles that microRNAs can play.

Our findings show that *miR-14* controls this context-specific autophagy in dying salivary gland cells by targeting the IP3-kinase *ip3k2*. Although the percentage of animals with a defect in salivary gland clearance appears less severe in animals with compromised IP3/calcium signaling compared to *miR-14* mutant animals, this is most likely due to RNAi knockdown and IP3 sponge expression efficiencies. In addition, in all histological analyses of salivary gland clearance, there is an inherent range of salivary gland material appearance and size. For example, cellular fragments are detached from each other and therefore fluid. Thus, two dimensional histological sections do not always convey the best representation of salivary gland material in an animal.

To the best of our knowledge, no IP3-kinase has previously been implicated in the control of autophagy. Our data indicate that *ip3k2* regulates autophagy through IP3 signaling, by inducing the release of calcium, thereby affecting Calmodulin activity. Our findings imply that calcium-bound Calmodulin activity should result in the induction of autophagy, potentially through the modulation of proteins such as Calmodulin-dependent kinases and/or Atg proteins. A previous study demonstrated that Calmodulin can bind IP3K2 *in vitro*, and that this calcium-dependent binding decreased the ability of IP3K2 to remove IP3 (Lloyd-Burton et al., 2007). It is possible that calcium released by IP3 signaling could activate Calmodulin, resulting in a positive feedback loop to inhibit IP3K2, releasing more calcium to activate Calmodulin further, and induce higher levels of autophagy that contribute to salivary gland cell death.

Interestingly, *ip3k1* is also a predicted target of *miR-14*, but we observed no influence of this gene on autophagy in the salivary gland using two independent RNAi lines that target distinct sequences (Table S2) (Terhzaz et al., 2010). Additionally, heterozygous loss of *ip3k1* failed to suppress the *miR-14* salivary gland clearance defect (data not shown), suggesting that *ip3k1* is not involved in the regulation of autophagy during salivary gland death. Furthermore, a previous study demonstrated that Calmodulin cannot bind IP3K1 *in vitro* (Lloyd-Burton et al., 2007), and it may be this lack of interaction that ensures that IP3K1 does not regulate autophagy during salivary gland destruction.

While multiple studies have linked calcium signaling to autophagy (Decuypere et al., 2011), the manner, either positive or negative, in which calcium influences autophagy seems to depend on context. Since it has been shown that a rise in free Ca2+ can induce autophagy via mTOR inhibition (Høyer-Hansen et al., 2007), it is possible that the mTOR pathway could contribute to the effect of *miR-14* on autophagy induction. However, we have previously shown that that modulation of mTOR pathway influences both cell size and tGPH reporter localization (Berry and Baehrecke, 2007). Since neither cell size nor tGPH reporter were affected in *mir-14* mutant salivary glands (Figure 2A and 2B), it appears unlikely that mTOR activity is appreciably altered by loss of *mir-14*.

Finally, we cannot exclude that *ip3k2* could also regulate autophagy in an IP3- and/or calcium-independent manner. For example, the mammalian Beclin1 (Atg6) complex has been shown to bind the ER localized IP3-receptor through the protein NAF-1 (Chang et al., 2010). Therefore, it is possible that IP3 signaling may serve as a mechanism to relocate the Beclin1 complex to the ER so that the ER can function as a membrane source for autophagosomes. Additionally, calcium signaling may cooperate with localization of the Beclin1 complex to the ER to achieve complete induction of autophagy during salivary gland cell death. Future studies should resolve how *miR-14* and its target, the novel autophagy factor *ip3k2*, and IP3 signaling regulate autophagy.

EXPERIMENTAL PROCEDURES

Drosophila strains

See supplemental experimental procedures.

ip3k2$^{\Delta 1}$ mutant

The *ip3k2*$^{\Delta 1}$ deletion allele was created by flippase mediated site specific recombination of two transposable p-element strains containing flippase recognition target sequences. For more details see supplemental experimental procedures.

Transgenic strains

To generate the *tub*-eGFP-*ip3k2* wild type 3′UTR vector, the 3′UTR of *ip3k2* was PCR amplified from genomic DNA. The *miR-14* binding site was mutated via *de novo* gene synthesis (Biomatik). Construct sequences were validated and inserted into the attP2 landing site to generate transgenic *Drosophila* lines (Genetic Services, Inc). For more details see supplemental experimental procedures.

Quantitative real-time PCR

RNA isolated from staged salivary glands was performed as described previously (Andres and Thummel, 1994). Five μL of a 0.5ng/μL RNA sample was used for multiplex miR-Taqman reactions according to the manufacturer's instruction, using an ABI 7900HT Real Time PCR System (Applied Biosystems).

Protein Extracts and Western Blotting

Protein extraction and Western Blotting were performed as described previously (Dutta and Baehrecke, 2008). Primary antibodies used were rabbit anti-GFP (1:1,000) (Novus Biologicals), chicken anti-GFP (1:20,000) (Abcam), mouse anti-Ecdysone Receptor (1:500) (Developmental Studies Hybridoma Bank), mouse anti-Broad Complex (1:100) (Developmental Studies Hybridoma Bank), Rabbit anti-Histone-H3 (1:2000) (Santa Cruz Biotechnology), and mouse anti-Beta-Tubulin (1:500) (Developmental Studies Hybridoma Bank). Western blots were imaged using a Bio-Rad Chemi-Doc XRS+ and quantified using Bio-Rad Image Lab software.

Histology

Histology was performed as described previously (Muro et al., 2006).

Immunolabeling and Microscopy

For immunohistochemisty, salivary glands were dissected from animals kept at 25°C, fixed in 4% paraformaldehyde (PFA) overnight at 4°C, blocked in PBS, 1% BSA and 0.1% tween (PBSBT), and incubated with rabbit anti-cleaved-Caspase-3 (1:400) (Cell Signaling Technology) overnight at 4°C. Salivary glands were washed for two hours at room temperature in PBSBT, incubated with appropriate secondary antibodies for two hours at room temperature, and washed for one hour in PBSBT. Salivary glands were mounted in Vectashield (Vector Laboratories). For mCherry-Atg8a, tGPH and cell size analyses, salivary glands were dissected from animals staged at 25°C, fixed in 2% PFA containing 2μM Hoechst stain for two minutes at room temperature, washed in PBS, and mounted in PBS. Cell size was measured using Zeiss measure software. mCherry-Atg8a puncta were quantified using Zeiss Automeasure software. Pixel intensity was measured using ImageJ software. All imaging except GCaMP was performed on a Zeiss Axiophot II microscope. GCaMP imaging was performed on a Zeiss two-photon microscope, LSM 7 MP. During all quantifications, the images that were used were unaltered. In all mCherry-Atg8a and cleaved-Caspase-3 figures, the brightness, contrast, and gamma were altered separately from the DNA to better emphasize puncta.

Induction of cell clones

The induction of mis-expression and RNAi-expressing cell clones was performed as described previously (McPhee et al., 2010).

Starvation of larvae

Starvation of larvae was performed as described previously (McPhee et al., 2010).

Supplementary Material

Refer to Web version on PubMed Central for supplementary material.

Acknowledgments

We thank R. Carthew, S. Cohen, F.-B. Gao, B. Hay, L. Johnston, E. Lai, N. Sokol, P. Zamore, L. Zipursky, the Bloomington Stock Center, the *Drosophila* Genetic Resource Center, and the VDRC for flies and reagents, and S. Gupta, T. Fortier and R. Lee for technical support. This work was supported by NIH grants R01GM34028 to V.A. and GM079431 and GM079431-04S1 to E.H.B. V.A. and E.H.B. are Ellison Medical Foundation Scholars, and are members of the UMass DERC (DK32520).

References

Akerboom J, Chen TW, Wardill TJ, Tian L, Marvin JS, Mutlu S, Calderón NC, Esposti F, Borghuis BG, Sun XR, et al. Optimization of a GCaMP calcium indicator for neural activity imaging. J Neurosci. 2012; 32:13819–13840. [PubMed: 23035093]

Ambros V. MicroRNAs and developmental timing. Curr Opin Genet Dev. 2011; 21:511–517. [PubMed: 21530229]

Andres, AJ.; Thummel, CS. Methods for quantitative analysis of transcription in larvae and prepupae*Drosophila melanogaster*: Practical Uses in Cell and Molecular Biology. Goldstein, L.; Fyrberg, E., editors. New York: Academic Press; 1994. p. 565-573.

Berridge MJ, Lipp P, Bootman MD. The versatility and universality of calcium signalling. Nat Rev Mol Cell Biol. 2000; 1:11–21. [PubMed: 11413485]

Berry DL, Baehrecke EH. Growth arrest and autophagy are required for salivary gland cell degradation in *Drosophila*. Cell. 2007; 131:1137–1148. [PubMed: 18083103]

Brennecke J, Hipfner DR, Stark A, Russell RB, Cohen SM. *bantam* encodes a developmentally regulated microRNA that controls cell proliferation and regulates the proapoptotic gene *hid* in *Drosophila*. Cell. 2003; 113:25–36. [PubMed: 12679032]

Britton JS, Lockwood WK, Li L, Cohen SM, Edgar BA. Drosophila's insulin/PI3-kinase pathway coordinates cellular metabolism with nutritional conditions. Dev Cell. 2002; 2:239–249. [PubMed: 11832249]

Caygill EE, Johnston LA. Temporal regulation of metamorphic processes in Drosophila by the let-7 and miR-125 heterochronic microRNAs. Curr Biol. 2008; 18:943–950. [PubMed: 18571409]

Cayirlioglu P, Kadow IG, Zhan X, Okamura K, Suh GS, Gunning D, Lai EC, Zipursky SL. Hybrid neurons in a microRNA mutant are putative evolutionary intermediates in insect CO2 sensory systems. Science. 2008; 319:1256–1260. [PubMed: 18309086]

Chang NC, Nguyen M, Germain M, Shore GC. Antagonism of Beclin 1-dependent autophagy by BCL-2 at the endoplasmic reticulum requires NAF-1. EMBO J. 2010; 29:606–618. [PubMed: 20010695]

Chang TK, Shravage BV, Hayes SD, Powers CM, Simin RT, Harper JW, Baehrecke EH. Uba1 functions in Atg7- and Atg3-independent autophagy. Nat Cell Biol. 2013; 15:1067–1078. [PubMed: 23873149]

Decuypere JP, Bultynck G, Parys JB. A dual role for Ca(2+) in autophagy regulation. Cell Calcium. 2011; 50:242–250. [PubMed: 21571367]

Denton D, Chang TK, Nicolson S, Shravage B, Simin R, Baehrecke EH, Kumar S. Relationship between growth arrest and autophagy in midgut programmed cell death in Drosophila. Cell Death Differ. 2012; 19:1299–1307. [PubMed: 22555456]

Dutta S, Baehrecke EH. Warts is required for PI3K-regulated growth arrest, autophagy, and autophagic cell death in Drosophila. Curr Biol. 2008; 18:1466–1475. [PubMed: 18818081]

Frankel LB, Wen J, Lees M, Høyer-Hansen M, Farkas T, Krogh A, Jäättelä M, Lund AH. microRNA-101 is a potent inhibitor of autophagy. EMBO J. 2011; 30:4628–4641. [PubMed: 21915098]

Gauhar Z, Sun LV, Hua S, Mason CE, Fuchs F, Li TR, Boutros M, White KP. Genomic mapping of binding regions for the Ecdysone receptor protein complex. Genome Res. 2009; 19:1006–1013. [PubMed: 19237466]

Gibbings D, Mostowy S, Jay F, Schwab Y, Cossart P, Voinnet O. Selective autophagy degrades DICER and AGO2 and regulates miRNA activity. Nat Cell Biol. 2012; 14:1314–1321. [PubMed: 23143396]

Groth AC, Fish M, Nusse R, Calos MP. Construction of transgenic Drosophila by using the site-specific integrase from phage phiC31. Genetics. 2004; 166:1775–1782. [PubMed: 15126397]

Hay BA, Wolff T, Rubin GM. Expression of baculovirus P35 prevents cell death in *Drosophila*. Development. 1994; 120:2121–2129. [PubMed: 7925015]

Høyer-Hansen M, Bastholm L, Szyniarowski P, Campanella M, Szabadkai G, Farkas T, Bianchi K, Fehrenbacher N, Elling F, Rizzuto R, et al. Control of macroautophagy by calcium, calmodulin-dependent kinase kinase-beta, and Bcl-2. Mol Cell. 2007; 25:193–205. [PubMed: 17244528]

Jiang C, Baehrecke EH, Thummel CS. Steroid regulated programmed cell death during *Drosophila* metamorphosis. Development. 1997; 124:4673–4683. [PubMed: 9409683]

Karres JS, Hilgers V, Carrera I, Treisman J, Cohen SM. The conserved microRNA miR-8 tunes atrophin levels to prevent neurodegeneration in Drosophila. Cell. 2007; 131:136–145. [PubMed: 17923093]

Lee CY, Baehrecke EH. Steroid regulation of autophagic programmed cell death during development. Development. 2001; 128:1443–1455. [PubMed: 11262243]

Li X, Carthew RW. A microRNA mediates EGF receptor signaling and promotes photoreceptor differentiation in the Drosophila eye. Cell. 2005; 123:1267–1277. [PubMed: 16377567]

Li Y, Wang F, Lee JA, Gao FB. MicroRNA-9a ensures the precise specification of sensory organ precursors in Drosophila. Genes Dev. 2006; 20:2793–2805. [PubMed: 17015424]

Lloyd-Burton SM, Yu JC, Irvine RF, Schell MJ. Regulation of inositol 1,4,5-trisphosphate 3-kinases by calcium and localization in cells. J Biol Chem. 2007; 282:9526–9535. [PubMed: 17284449]

Martin DN, Baehrecke EH. Caspases function in autophagic cell death in *Drosophila*. Development. 2004; 131:275–284. [PubMed: 14668412]

McPhee CK, Logan MA, Freeman MR, EHB. Activation of autophagy during cell death requires the engulfment receptor Draper. Nature. 2010; 465:1093–1096. [PubMed: 20577216]

Mizushima N, Komatsu M. Autophagy: Renovation of Cells and Tissues Cell. 2011; 147:728–741.

Muro I, Berry DL, Huh JR, Chen CH, Huang H, Yoo SJ, Guo M, Baehrecke EH, Hay BA. The Drosophila caspase Ice is important for many apoptotic cell deaths and for spermatid individualization, a nonapoptotic process. Development. 2006; 133:3305–3315. [PubMed: 16887831]

Seeds AM, Sandquist JC, Spana EP, York JD. A molecular basis for inositol polyphosphate synthesis in Drosophila melanogaster. J Biol Chem. 2004; 279:47222–47232. [PubMed: 15322119]

Sokol NS. Small temporal RNAs in animal development. Curr Opin Genet Dev. 2012; 22:368–373. [PubMed: 22578317]

Sokol NS, Xu P, Jan YN, Ambros V. Drosophila let-7 microRNA is required for remodeling of the neuromusculature during metamorphosis. Genes Dev. 2008; 22:1591–1596. [PubMed: 18559475]

Teleman AA, Maitra S, Cohen SM. Drosophila lacking microRNA miR-278 are defective in energy homeostasis. Genes Dev. 2006; 20:417–422. [PubMed: 16481470]

Terhzaz S, Finlayson AJ, Stirrat L, Yang J, Tricoire H, Woods DJ, Dow JA, Davies SA. Cell-specific inositol 1,4,5 trisphosphate 3-kinase mediates epithelial cell apoptosis in response to oxidative stress in Drosophila. Cell Signal. 2010; 22:737–748. [PubMed: 20060894]

Usui-Aoki K, Matsumoto K, Koganezawa M, Kohatsu S, Isono K, Matsubayashi H, Yamamoto MT, Ueda R, Takahashi K, Saigo K, et al. Targeted expression of Ip3 sponge and Ip3 dsRNA impaires sugar taste sensation in Drosophila. J Neurogenet. 2005; 19:123–141. [PubMed: 16540404]

Varghese J, Cohen SM. microRNA miR-14 acts to modulate a positive autoregulatory loop controlling steroid hormone signaling in Drosophila. Genes Dev. 2009; 21:2277–2282. [PubMed: 17761811]

Varghese J, Lim SF, Cohen SM. Drosophila miR-14 regulates insulin production and metabolism through its target, sugarbabe. Genes Dev. 2010; 24:2748–2753. [PubMed: 21159815]

Xu P, Vernooy SY, Guo M, Hay BA. The *Drosophila* microRNA mir-14 suppresses cell death and is required for normal fat metabolism. Curr Biol. 2003; 13:790–795. [PubMed: 12725740]

Zhang P, Zhang H. Autophagy modulates miRNA-mediated gene silencing and selectively degrades AIN-1/GW182 in C. elegans. EMBO Rep. 2013; 14:568–576. [PubMed: 23619095]

Zhu H, Wu H, Liu X, Li B, Chen Y, Ren X, Liu CG, Yang JM. Regulation of autophagy by a beclin 1-targeted microRNA, miR-30a, in cancer cells. Autophagy. 2009; 5:816–823. [PubMed: 19535919]

HIGHLIGHTS

- *miR-14* is necessary and sufficient for autophagy during cell death
- *miR-14* targets the *inositol 1,4,5-trisphosphate kinase 2* gene to regulate autophagy
- IP3 signaling and *Calmodulin* are necessary for autophagy during cell death
- *miR-14* regulates calcium levels during salivary gland destruction

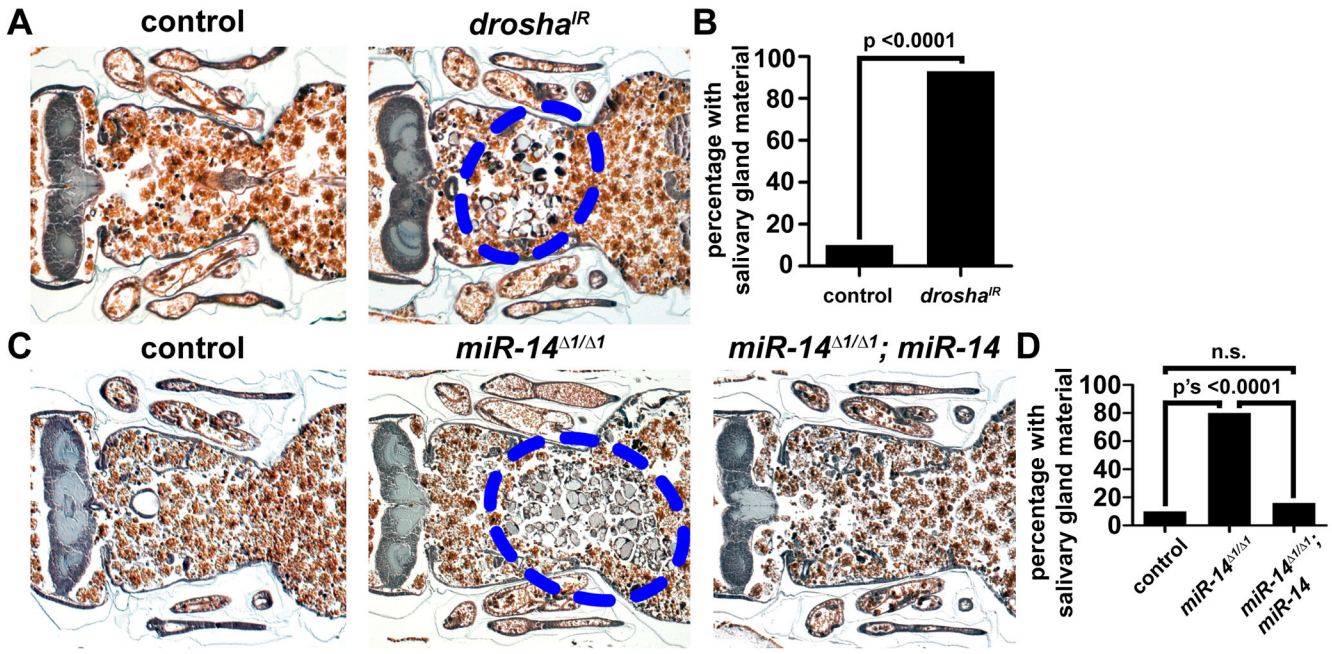

Figure 1. *Drosha* and *miR-14* are required for salivary gland degradation

(A) Samples from control animals (*+/w; +*/UAS-*drosha*^{IR}), *n* = 16 (left), and those with salivary gland-specific knockdown of *drosha* (*fkh*-GAL4/*w*; +/UAS-*drosha*^{IR}), *n* = 27 (right), analyzed by histology for the presence of salivary gland material (blue dotted circle) 24 h after puparium formation.

(B) Quantification of data from (A). Data are represented as mean. Statistical significance was determined using a Chi-squared test.

(C) Samples from control animals (*w*; +/*miR-14*$^{\Delta 1}$; *fkh*-GAL4/UAS-*luciferase-miR-14*), *n* = 39 (left), *miR-14* null mutants (*w; miR-14*$^{\Delta 1}$/*miR-14*$^{\Delta 1}$; +/UAS-*luciferase-miR-14*), *n* = 25 (middle), and *miR-14* null mutants with salivary gland-specific expression of *miR-14* (*w; miR-14*$^{\Delta 1}$/*miR-14*$^{\Delta 1}$; *fkh*-GAL4/UAS-*luciferase-miR-14*), *n* = 25 (right), analyzed by histology for the presence of salivary gland material (blue dotted circle) 24 h after puparium formation.

(D) Quantification of data from (C). Data are represented as mean. Statistical significance was determined using a Chi-squared test.

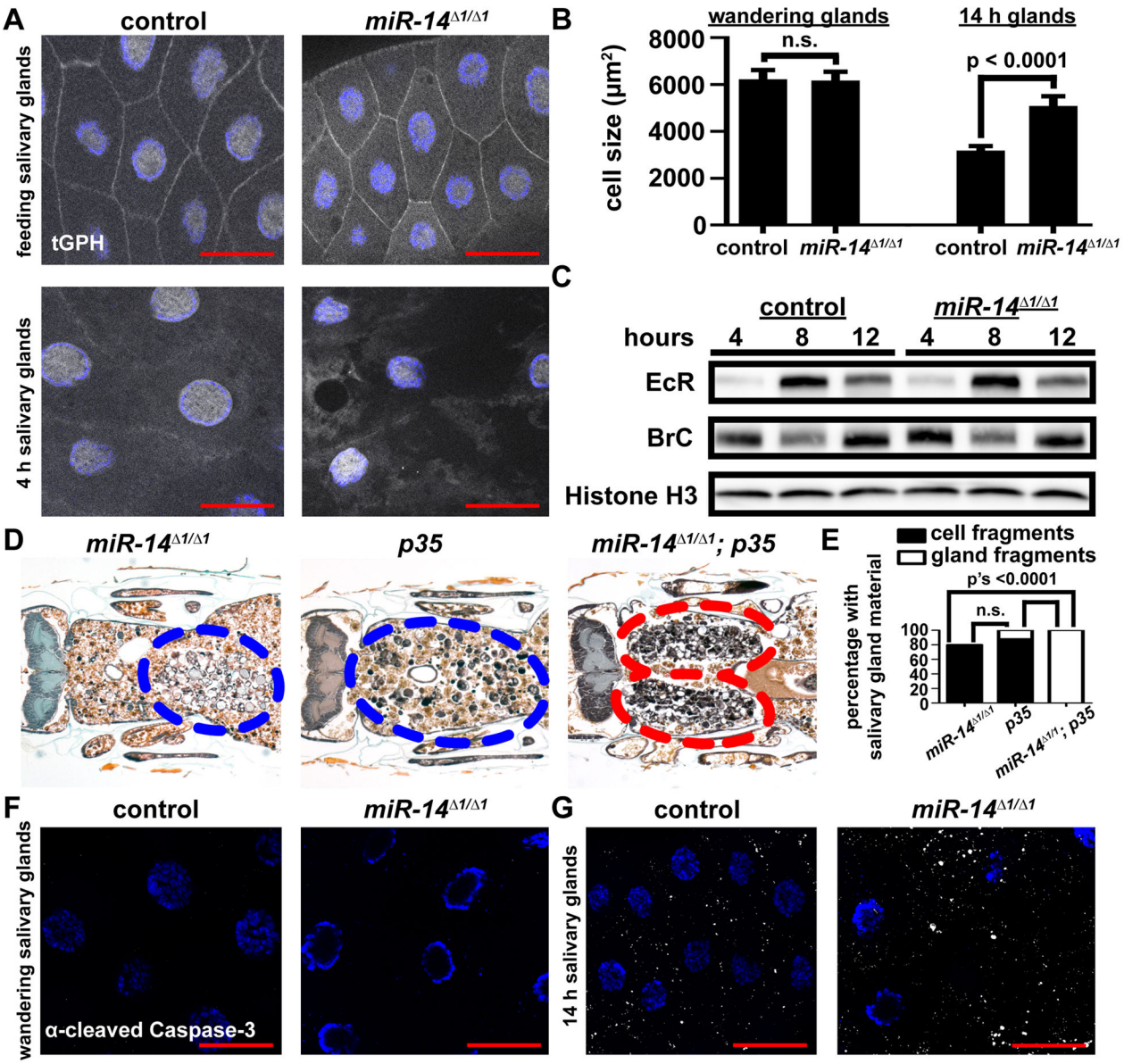

Figure 2. Loss of *miR-14* does not alter cell growth, hormone signaling, or caspase activity during salivary gland degradation

(A) Salivary glands dissected from control (+/*w*; +/*miR-14*$^{\Delta 1}$, tGPH) and *miR-14* null mutant (*w; miR-14*$^{\Delta 1}$/*miR-14*$^{\Delta 1}$, tGPH) animals as feeding larvae (top) and 4 h after puparium formation (bottom) for analysis of tGPH localization. Salivary glands were all stained with Hoechst (blue). Scale bars represent 50μm.

(B) Salivary gland cell size in control (+/*w*; +/*miR-14*$^{\Delta 1}$), $n \geq 32$, and *miR-14* null mutant (*w; miR-14*$^{\Delta 1}$/*miR-14*$^{\Delta 1}$), $n \geq 29$, animals dissected from wandering larvae and 14 h after puparium formation. Statistical significance was determined using a Student's t-test. Data are represented as mean +/− SEM.

(C) Protein extracts from salivary glands 4, 8 and 12 hours after puparium formation of control (+/*w*; +/*miR-14*$^{\Delta 1}$) and *miR-14* null mutant (*w; miR-14*$^{\Delta 1}$/*miR-14*$^{\Delta 1}$) animals

analyzed by immuno-blot with anti-Ecdysone Receptor (EcR) and anti-Broad Complex (BR-C).

(D) Samples from *miR-14* null mutants (*w; miR-14*$^{\Delta 1}$/*miR-14*$^{\Delta 1}$; UAS-p35/+), *n* = 20 (left), animals with salivary gland-specific expression of p35 (*w; miR-14*$^{\Delta 1}$/+; UAS-p35/*fkh*-GAL4), *n* = 26 (middle), and *miR-14* null mutants with salivary gland-specific expression of p35 (*w; miR-14*$^{\Delta 1}$/*miR-14*$^{\Delta 1}$; UAS-p35/*fkh*-GAL4), *n* = 24 (right), analyzed by histology for the presence of salivary gland material 24 h after puparium formation. Blue dotted circles enclose cell fragments; red dotted circles enclose gland fragments.

(E) Quantification of data from (D). Data are represented as mean. Statistical significance was determined using a Chi-squared test comparing the percentages of gland fragments. (F and G) Salivary glands dissected from control (+/*w*; +/*miR-14*$^{\Delta 1}$) and *miR-14* null mutant (*w; miR-14*$^{\Delta 1}$/*miR-14*$^{\Delta 1}$) animals and stained with cleaved Caspase-3 antibody (white) and Hoechst (blue). Salivary glands were dissected from wandering larvae (F) and 14 h after puparium formation (G). Scale bars represent 50 μm.

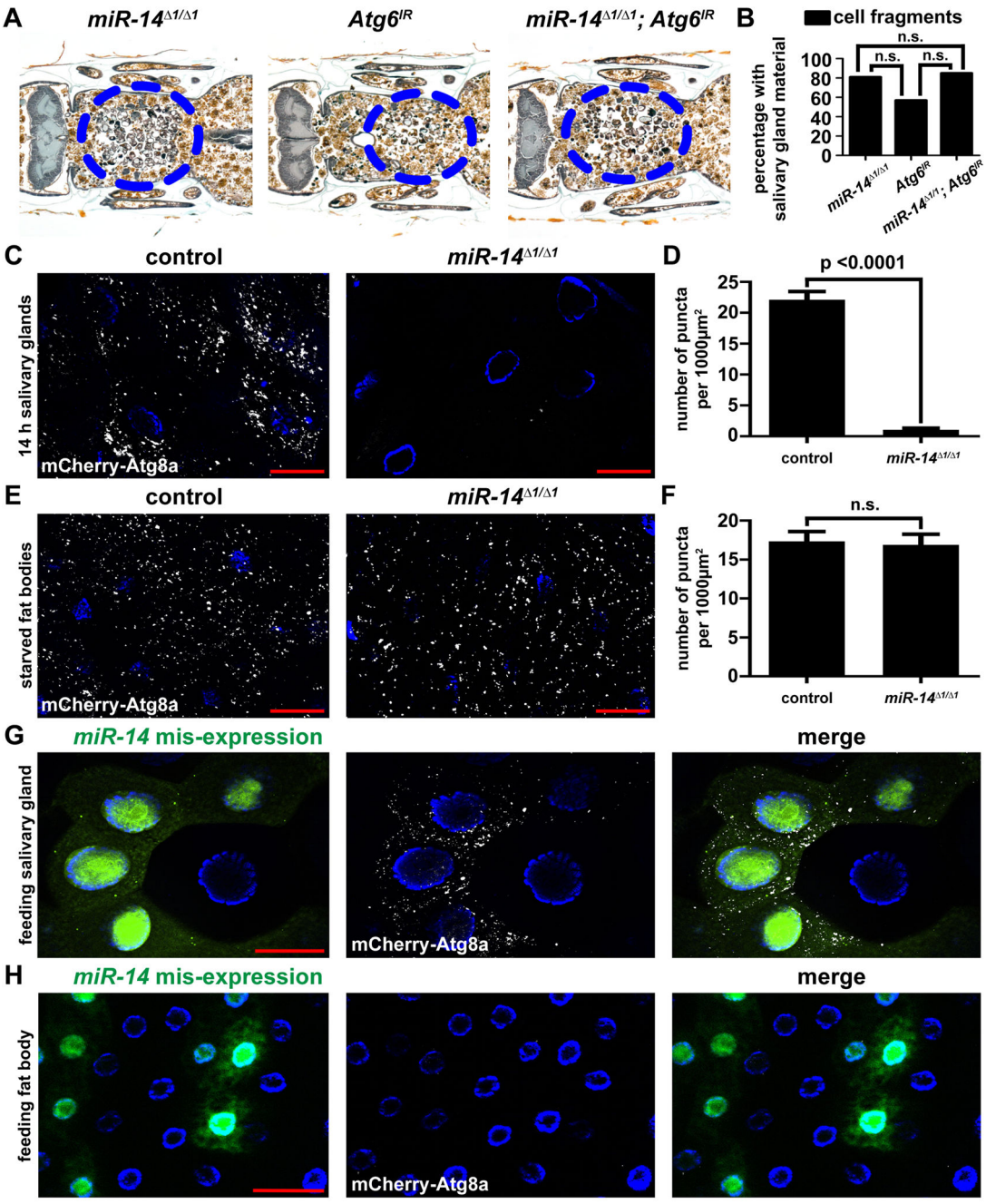

Figure 3. *miR-14* is necessary and sufficient for autophagy in salivary glands, but not fat body

(A) Samples from *miR-14* null mutants (*w; miR-14*$^{\Delta 1}$/*miR-14*$^{\Delta 1}$; UAS-*Atg6*^{IR}/+), *n* = 24 (left), animals with salivary gland-specific knockdown of *Atg6* (*w; miR-14* $^{\Delta 1}$/+; UAS-*Atg6*^{IR}/*fkh*-GAL4), *n* = 21 (middle), and *miR-14* null mutants with salivary gland-specific knockdown of *Atg6* (*w; miR-14*$^{\Delta 1}$/*miR-14*$^{\Delta 1}$; UAS-*Atg6*^{IR}/*fkh*-GAL4), *n* = 24 (right), analyzed by histology for the presence of salivary gland material 24 h after puparium formation. Blue dotted circles enclose cell fragments.

(B) Quantification of data from (A). Data are represented as mean. Statistical significance was determined using a Chi-squared test comparing the percentages of animals with gland fragments.

(C) mCherry-Atg8a was expressed in the salivary glands of control animals (+/*w*; +/pmCherry-Atg8a, *miR-14*$^{\Delta 1}$) and in *miR-14* null mutants (*w*; pmCherry-Atg8a, *miR-14*$^{\Delta 1}$/*miR-14*$^{\Delta 1}$). Salivary glands were dissected 14 h after puparium formation for analyses of mCherry-Atg8a puncta.

(D) Quantification of data from (C). Data are represented as mean +/− SEM; $n \geq 23$. Statistical significance was determined using a Student's t-test.

(E) mCherry-Atg8a was expressed in the fat bodies of control animals (+/*w*; +/pmCherry-Atg8a, *miR-14*$^{\Delta 1}$) and in *miR-14* null mutants (*w*; pmCherry-Atg8a, *miR-14* $^{\Delta 1}$/*miR-14*$^{\Delta 1}$). Larvae were starved for 4 h, and fat bodies were dissected for analyses of mCherry-Atg8a puncta.

(F) Quantification of data from (E). Data are represented as mean +/− SEM; $n \geq 19$. Statistical significance was determined using a Student's t-test.

(G and H) Salivary glands (G) and fat bodies (H) expressing mCherry-Atg8a in all cells, and *miR-14* mis-expression specifically in GFP-marked clone cells (heatshock (hs)flp/*w*; pmCherry-Atg8a/UAS-*miR-14; act*<FRT, cd2, FRT>Gal4, UAS-GFP/+) dissected from feeding larvae for analyses of mCherry-Atg8a puncta. Salivary glands and fat bodies were all stained with Hoechst (blue). Scale bars represent 50 μm.

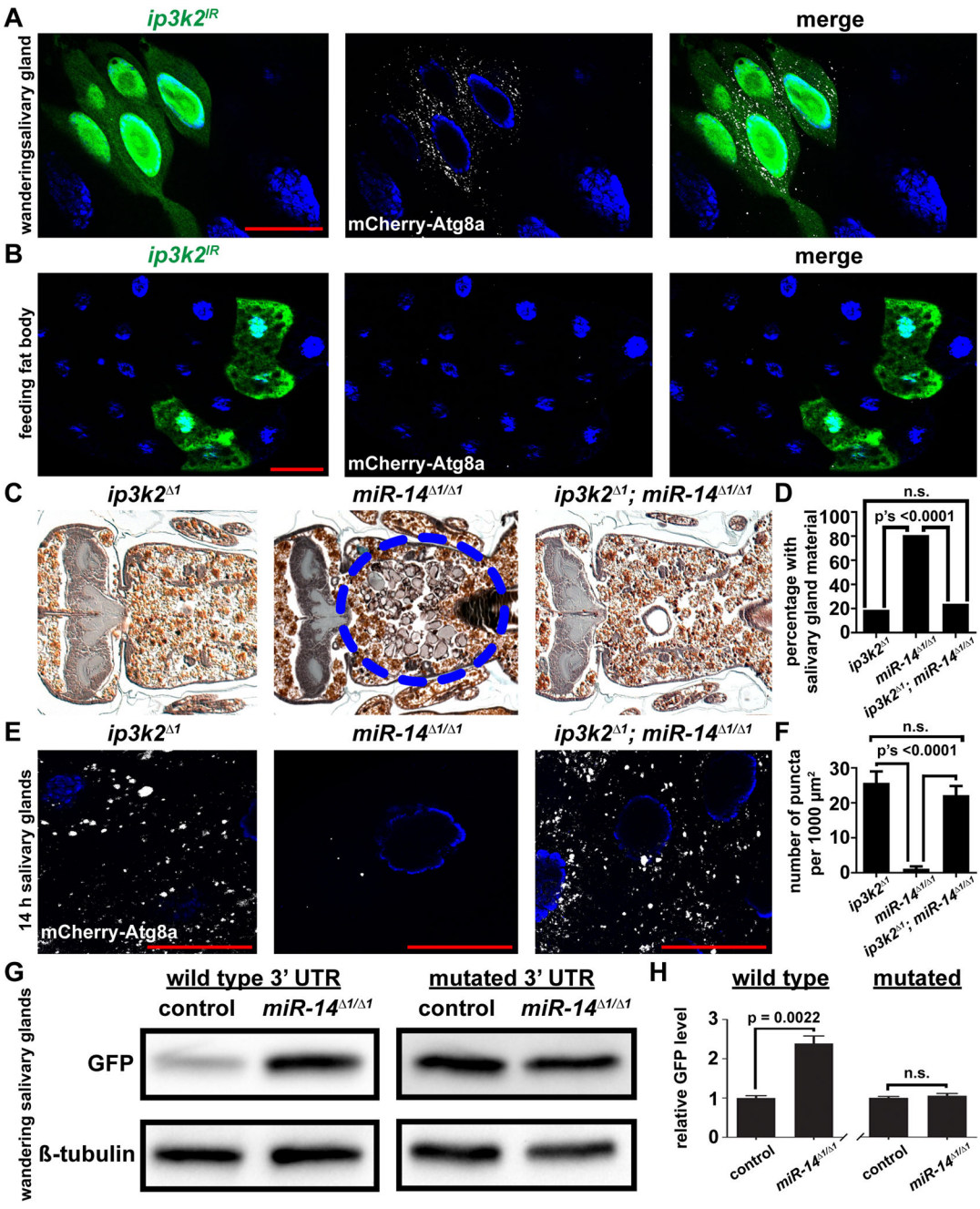

Figure 4. *miR-14* targets *inositol 1,4,5-trisphosphate kinase 2* to regulate autophagy during salivary gland death

(A and B) Salivary glands dissected from wandering larvae (A) and fat bodies dissected from feeding larvae (B) expressing mCherry-Atg8a in all cells, and *ip3k2* knockdown specifically in GFP-marked clone cells (hsflp/*w*; pmCherry-Atg8a/UAS-*ip3k2*^{IR}; *act*<FRT, cd2, FRT>Gal4, UAS-GFP/+) analyzed for mCherry-Atg8a puncta.

(C) Samples from *ip3k2* mutant animals (*ip3k2* $^{\Delta 1}$/Y; +/*miR-14*$^{\Delta 1}$), *n* = 21 (left), *miR-14* null mutant animals (*ip3k2* $^{\Delta 1}$/*w*; *miR-14*$^{\Delta 1}$/*miR-14*$^{\Delta 1}$), *n* = 26 (middle), and *ip3k2*, *miR-14* double mutant animals (*ip3k2* $^{\Delta 1}$/Y; *miR-14*$^{\Delta 1}$/*miR-14*$^{\Delta 1}$), *n* = 50 (right), analyzed by

histology for the presence of salivary gland material (blue dotted circle) 24 h after puparium formation.

(D) Quantification of data from (C). Data are represented as mean. Statistical significance was determined using a Chi-squared test.

(E) mCherry-Atg8a was expressed in *ip3k2* mutant animals (*ip3k2* $^{\Delta 1}$/Y; *miR-14*$^{\Delta 1}$/ pmCherry-Atg8a), *miR-14* null mutant animals (*ip3k2* $^{\Delta 1}$/*w; miR-14*$^{\Delta 1}$/*miR-14*$^{\Delta 1}$, pmCherry-Atg8a), and *ip3k2*, *miR-14* null double mutant animals (*ip3k2* $^{\Delta 1}$/Y; *miR-14*$^{\Delta 1}$/*miR-14*$^{\Delta 1}$, pmCherry-Atg8a). Salivary glands were dissected 14 h after puparium formation for analyses of mCherry-Atg8a puncta.

(F) Quantification of data from (E). Data are represented as mean +/− SEM; $n \geq 16$. Statistical significance was determined using a Student's t-test. Salivary glands and fat bodies were all stained with Hoechst (blue). Scale bars represent 50 μm.

(G) Protein extracts from salivary glands dissected from wandering larvae of control (*w; miR-14*$^{\Delta 1}$/+; *tub*-GFP-*ip3k2* 3′UTR/+) and *miR-14* null mutant (*w; miR-14*$^{\Delta 1}$/*miR-14*$^{\Delta 1}$; *tub*-GFP-*ip3k2* 3′UTR/+) animals expressing a GFP sensor containing either the wild type *ip3k2* 3′UTR or a mutated *miR-14* binding site in the 3′UTR, and analyzed by immuno-blot with anti-GFP antibody.

(H) Quantification of data from (G). Wild type and mutated sensors are normalized to Beta-tubulin and plotted relative to their respective controls +/− SEM; *n*'s = 3. Statistical significance was determined using a Student's t-test.

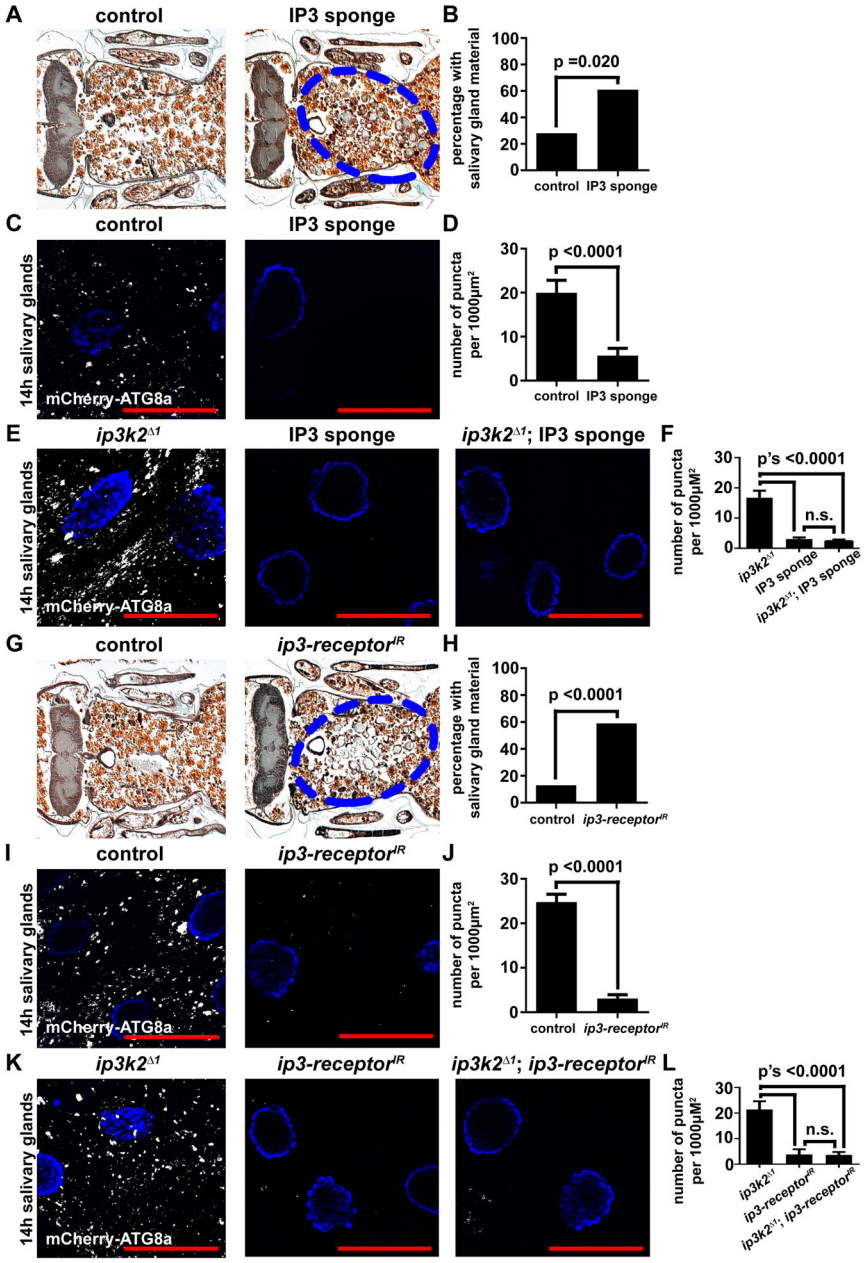

Figure 5. IP3 signaling functions downstream of *ip3k2* and is required for autophagy and the degradation of salivary glands

(A) Samples from control animals (*+/w; +*/UAS-IP3 sponge), *n* = 32 (left), and those with salivary gland-specific expression of the IP3 sponge (*fkh*-GAL4/*w*; +/UAS-IP3 sponge), *n* = 28 (right), analyzed by histology for the presence of salivary gland material (blue dotted circle) 24 h after puparium formation.

(B) Quantification of data from (A). Data are represented as mean. Statistical significance was determined using a Chi-squared test.

(C) mCherry-Atg8a was expressed in the salivary glands of control animals (*w;* +/ pmCherry-Atg8a; UAS-IP3 sponge/+) (left), and those with salivary gland-specific

expression of the IP3 sponge (*w*; pmCherry-Atg8a/+; *fkh*-GAL4/UAS-IP3 sponge) (right). Salivary glands were dissected 14 h after puparium formation for analyses of mCherry-Atg8a puncta.

(D) Quantification of data from (C). Data are represented as mean +/− SEM; $n \geq 11$. Statistical significance was determined using a Student's t-test.

(E) mCherry-Atg8a was expressed in *ip3k2* mutant animals (*ip3k2* $^{\Delta 1}$/Y; pmCherry-Atg8a/+; +/UAS-IP3 sponge), animals with salivary gland-specific expression of the IP3 sponge (*ip3k2* $^{\Delta 1}$/*w*; pmCherry-Atg8a/+; *fkh*-GAL4/UAS-IP3 sponge), and *ip3k2* mutant animals with salivary gland-specific expression of the IP3 sponge (*ip3k2* $^{\Delta 1}$/Y; pmCherry-Atg8a/+; *fkh*-GAL4/UAS-IP3 sponge). Salivary glands were dissected 14 h after puparium formation for analyses of mCherry-Atg8a puncta.

(F) Quantification of data from (E). Data are represented as mean +/− SEM; $n \geq 14$. Statistical significance was determined using a Student's t-test.

(G) Samples from control animals (*+/w; +/*UAS-*ip3-receptor*^{IR}), $n = 15$ (left), and those with salivary gland-specific knockdown of the *ip3-receptor* (*fkh*-GAL4/*w*; +/UAS-*ip3-receptor*^{IR}), $n = 27$ (right), analyzed by histology for the presence of salivary gland material (blue dotted circle) 24 h after puparium formation.

(H) Quantification of data from (G). Data are represented as mean. Statistical significance was determined using a Chi-squared test.

(I) mCherry-Atg8a was expressed in the salivary glands of control animals (*w;* UAS-*ip3-receptor*^{IR}/pmCherry-Atg8a) (left), and those with salivary gland-specific knockdown of the *ip3-receptor* (*w*; UAS-*ip3-receptor*^{IR}/pmCherry-Atg8a; +/*fkh*-GAL4) (right). Salivary glands were dissected 14 h after puparium formation for analyses of mCherry-Atg8a puncta.

(J) Quantification of data from (I). Data are represented as mean +/− SEM; $n \geq 21$. Statistical significance was determined using a Student's t-test.

(K) mCherry-Atg8a was expressed in *ip3k2* mutant animals (*ip3k2* $^{\Delta 1}$/Y; pmCherry-Atg8a/ UAS-*ip3-receptor*^{IR}), animals with salivary gland-specific knockdown of the *ip3-receptor* (*ip3k2* $^{\Delta 1}$/*w*; pmCherry-Atg8a/UAS-*ip3-receptor*^{IR}; *fkh*-GAL4/+), and *ip3k2* mutant animals with salivary gland-specific knockdown of the *ip3-receptor* (*ip3k2* $^{\Delta 1}$/Y; pmCherry-Atg8/ UAS-*ip3-receptor*^{IR}; *fkh*-GAL4/+). Salivary glands were dissected 14 h after puparium formation for analyses of mCherry-Atg8a puncta.

(L) Quantification of data from (K). Data are represented as mean +/− SEM; $n \geq 11$. Statistical significance was determined using a Student's t-test.

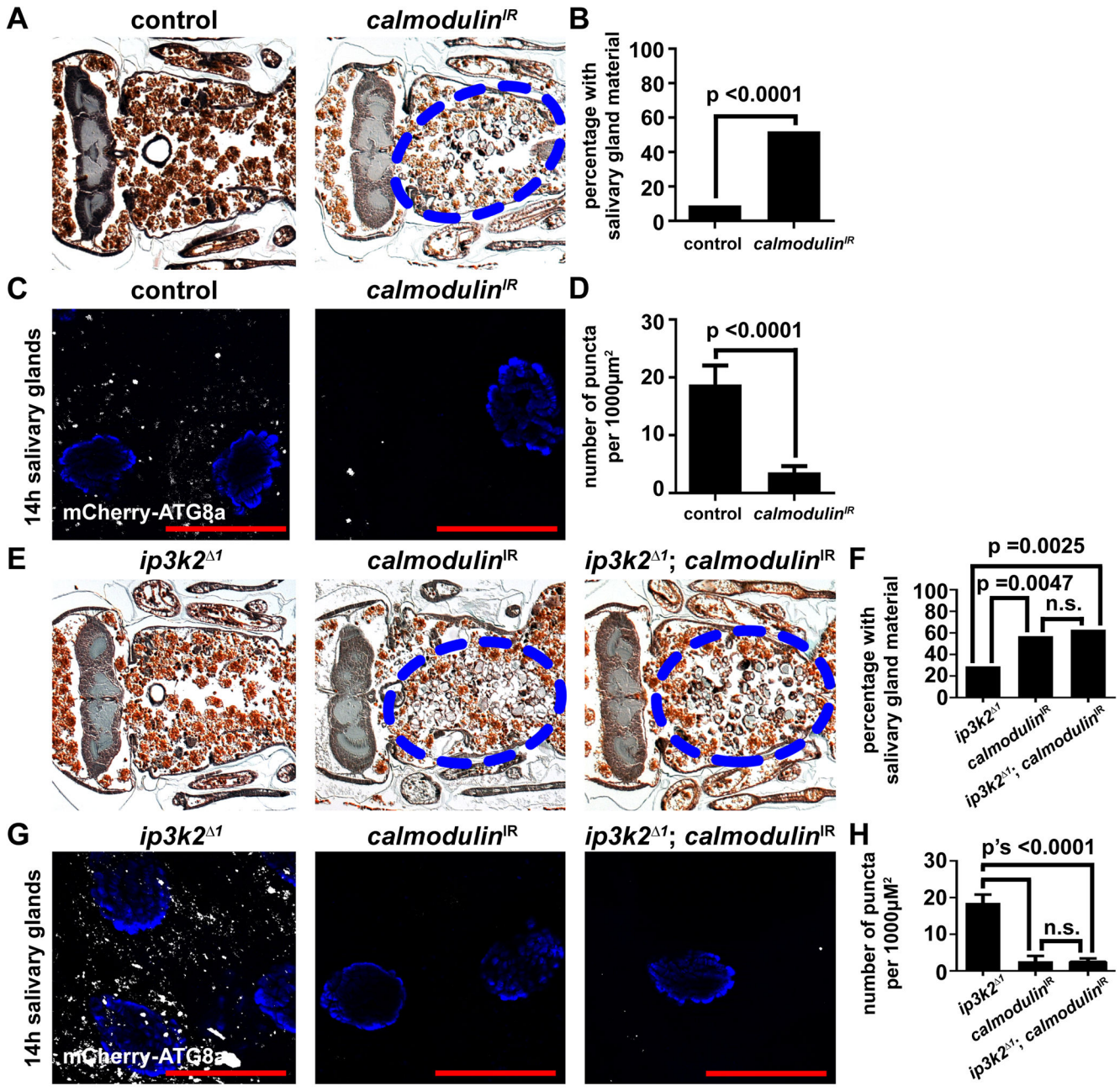

Figure 6. *Calmodulin* functions downstream of *ip3k2* and is required for autophagy and the degradation of salivary glands

(A) Samples from control animals (*+/w; +*/UAS-*Calmodulin*^{IR}), *n* = 22 (left), and those with salivary gland-specific knockdown of *Calmodulin* (*fkh*-GAL4/*w*; +/UAS-*Calmodulin*^{IR}), *n* = 29 (right), analyzed by histology for the presence of salivary gland material (blue dotted circle) 24 h after puparium formation.

(B) Quantification of data from (A). Data are represented as mean. Statistical significance was determined using a Chi-squared test.

(C) mCherry-Atg8a was expressed in the salivary glands of control animals (*w;* pmCherry-Atg8a/+; +/UAS-*Calmodulin*^{IR}) (left), and those with salivary gland-specific knockdown of

Calmodulin (*w*; pmCherry-Atg8a/+; *fkh*-GAL4/UAS-*Calmodulin*^{IR}) (right). Salivary glands were dissected 14 h after puparium formation for analyses of mCherry-Atg8a puncta.

(D) Quantification of data from (C). Data are represented as mean +/− SEM; $n \geq 15$. Statistical significance was determined using a Student's t-test. Salivary glands were all stained with Hoechst (blue). Scale bars represent 50 μm.

(E) Samples from *ip3k2* mutant animals (*ip3k2* $^{\Delta 1}$/Y; +/UAS-*Calmodulin*^{IR}), $n = 21$ (left), animals with salivary gland-specific knockdown of *Calmodulin* (*ip3k2* $^{\Delta 1}$/*w; fkh*-GAL4/UAS-*Calmodulin*^{IR}), $n = 28$ (middle), and *ip3k2* mutant animals with salivary gland-specific knockdown of *Calmodulin* (*ip3k2* $^{\Delta 1}$/Y; *fkh*-GAL4/UAS-*Calmodulin*^{IR}), $n = 24$ (right), analyzed by histology for the presence of salivary gland material (blue dotted circles) 24 h after puparium formation.

(F) Quantification of data from (E). Data are represented as mean. Statistical significance was determined using a Chi-squared test.

(G) mCherry-Atg8a was expressed in *ip3k2* mutant animals (*ip3k2* $^{\Delta 1}$/Y; pmCherry-Atg8a/+; +/UAS-*Calmodulin*^{IR}), animals with salivary gland-specific knockdown of *Calmodulin* (*ip3k2* $^{\Delta 1}$/*w*; +/pmCherry-Atg8a; *fkh*-GAL4/UAS-*Calmodulin*^{IR}), and *ip3k2* mutant animals with salivary gland-specific knockdown of *Calmodulin* (*ip3k2* $^{\Delta 1}$/Y; pmCherry-Atg8a/+; *fkh*-GAL4/UAS-*Calmodulin*^{IR}). Salivary glands were dissected 14 h after puparium formation for analyses of mCherry-Atg8a puncta.

(H) Quantification of data from (G). Data are represented as mean +/− SEM; $n \geq 10$. Statistical significance was determined using a Student's t-test. Salivary glands were all stained with Hoechst (blue). Scale bars represent 50 μm.

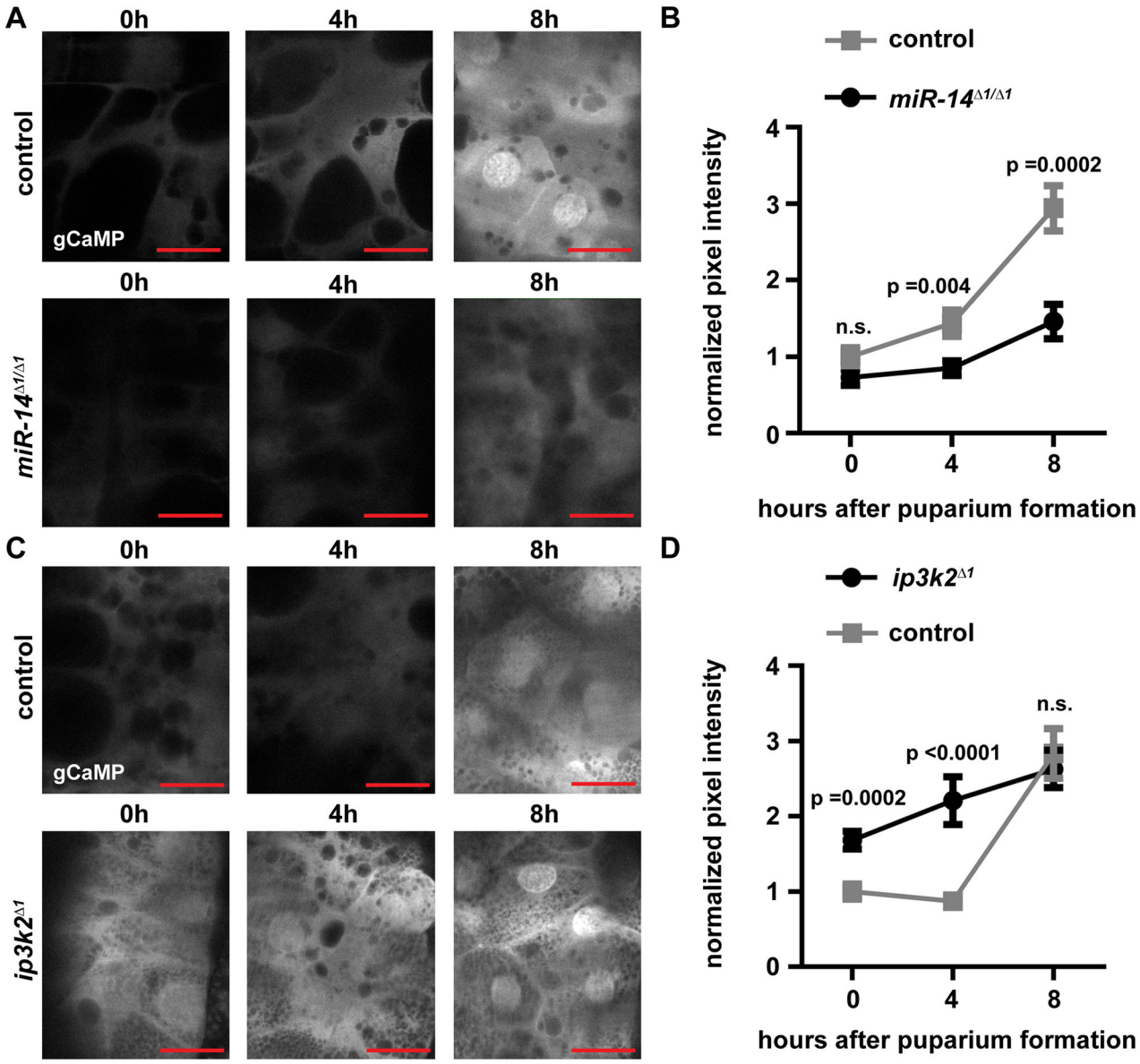

Figure 7. *miR-14* and *ip3k2* influence calcium levels in the salivary gland

(A) GCaMP was expressed specifically in the salivary glands of control animals (*w*; +/*miR-14*$^{\Delta 1}$; *fkh*-GAL4/UAS-GCaMP5) and *miR-14* mutant animals (*w; miR-14*$^{\Delta 1}$/*miR-14*$^{\Delta 1}$; *fkh*-GAL4/UAS-GCaMP5), and live-imaged at 0, 4 and 8 h after puparium formation.

(B) Quantification of data from (A). Statistical significance was determined using a Student's t-test. Error bars represent SEM; $n \geq 8$. Scale bars represent 50 μm.

(C) GCaMP was expressed specifically in the salivary glands of control animals (*ip3k2* $^{\Delta 1}$/*w*; +/UAS-GCaMP5; +/*fkh*-GAL4) and *ip3k2* mutant animals (*ip3k2* $^{\Delta 1}$/Y; +/UAS-GCaMP5; +/*fkh*-GAL4), and live-imaged at 0, 4 and 8 h after puparium formation.

(D) Quantification of data from (C). Statistical significance was determined using a Student's t-test. Error bars represent SEM; $n \geq 10$. Scale bars represent 50 μm. *miR-14* and *ip3k2* experiments are normalized to their respective controls.